

## Generation of Tunable 10-mJ-Level Terahertz Pulses through Nonlinear Plasma Wakefield Modulation

Hanqi Feng,<sup>1</sup> Zheng Zhou<sup>1</sup>,<sup>✉</sup> Yipeng Wu,<sup>1,2,\*</sup> Zhangfeng Gao,<sup>3,4</sup> Yifan Liang,<sup>1</sup> Nanshun Huang,<sup>3,4</sup> Lixin Yan<sup>1</sup>,<sup>†</sup> Haixiao Deng<sup>3,5</sup>, Yingchao Du<sup>1</sup>, Renkai Li,<sup>1</sup> Wei Lu,<sup>1</sup> Wenhui Huang,<sup>1</sup> and Chuanxiang Tang<sup>1</sup>


<sup>1</sup>*Department of Engineering Physics, Tsinghua University, and Key Laboratory of Particle and Radiation Imaging (Tsinghua University), Ministry of Education, Beijing 100084, China*

<sup>2</sup>*University of California, Los Angeles, California 90095, USA*

<sup>3</sup>*Shanghai Institute of Applied Physics, Chinese Academy of Sciences, Shanghai 201800, China*

<sup>4</sup>*University of Chinese Academy of Sciences, Beijing 100049, China*

<sup>5</sup>*Shanghai Advanced Research Institute, Chinese Academy of Sciences, Shanghai 201210, China*

 (Received 5 February 2021; revised 16 March 2021; accepted 25 March 2021; published 21 April 2021)

High-density electron-bunch train–based tunable coherent terahertz radiation with a narrow spectral bandwidth is highly essential for many scientific applications. Here we propose a scheme to produce ultrahigh-peak-current (more than 10 kA) electron-bunch trains with tunable picosecond spacing for the generation of such terahertz sources. Passing through a plasma section and interacting with the self-excited nonlinear plasma wake, the beam gains a “sawtooth” energy modulation. By means of magnetic optics, it is then effectively converted into a beam density modulation forming microbunches with a high charge of up to a few nanocoulombs and a bunching factor as high as approximately 0.8. Tunable narrowband terahertz radiation with energy on the order of 10 mJ can be generated, which we show in both theoretical analyses and simulations via this process. This scheme can be realized in accelerator facilities with repetition rates on the order of kilohertz or even submegahertz, which provides great potential in modern science and related technologies.

DOI: [10.1103/PhysRevApplied.15.044032](https://doi.org/10.1103/PhysRevApplied.15.044032)

### I. INTRODUCTION

Tunable terahertz sources in the frequency range from 0.1 to 10 THz are in great demand for broad applications ranging from molecular spectroscopy to compact electron acceleration, medical imaging, and security [1–4]. During the past two decades, significant progress has been made in developing various terahertz sources. Among them, electron accelerator–based terahertz sources have attracted considerable interest worldwide since they have the potential to provide terahertz radiation with high spectral brightness, high peak power, high repetition rates, and a large tuning range. The key to generating coherent terahertz radiation in these facilities is the manipulation of the beam phase space to form microbunches with picosecond or subpicosecond spacing.

Several approaches have been proposed and studied for the generation of picosecond and subpicosecond bunching in electron beams, including directly modulating the drive

laser [5–9], transforming transverse modulation to a longitudinal distribution [10,11], using self-modulation instability in a linear plasma wake [12], converting energy modulation induced by wakefields in dielectric-lined or corrugated waveguides to density bunching [13–17], and transforming laser-induced energy modulation to a density distribution [18–21]. For coherent radiation, terahertz energy is proportional to the square of the product of the beam charge  $Q$  and the bunching factor  $b$ , where  $b$  is defined as  $b(k) = \int_{-\infty}^{\infty} I(z)e^{-ikz} dz / \int_{-\infty}^{\infty} I(z) dz$ , with the beam current distribution  $I$  and the modulation wave number  $k$ . To date, the typical terahertz energy experimentally obtained by these methods is on the order of microjoules due to relatively low  $Q$  or  $b$ . Through optimization,  $b$  can be increased to approximately 0.4 for a relatively-high-charge beam and the calculated terahertz energy can reach 1 mJ, as recently proposed and tested through simulations [21]. As the field rapidly expands, sources of terahertz radiation with energy on the order of 10 mJ are in high demand for numerous scientific applications, such as extreme terahertz science featuring nonlinear light-matter interactions [4,22,23], waveguide coupling–based terahertz electron accelerators and manipulators [1,24–27], and nonlinear

\* wuyipeng@ucla.edu

† yanlx@tsinghua.edu.cn

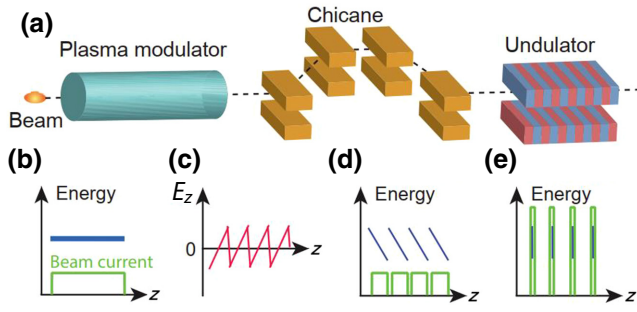


FIG. 1. (a) Layout of the proposed concept. (b) The beam longitudinal phase space and current distribution at the entrance of the plasma modulator. (c) The longitudinal wakefield  $E_z$  excited by the beam in the plasma. (d),(e) The beam longitudinal phase space and current distribution at the entrance and exit of the chicane, respectively.

terahertz bioeffect studies [28]. To achieve such high terahertz energy for a wide frequency range, a significant beam charge combined with a larger bunching factor is highly desired. However, it proves to be very challenging to meet these requirements at the same time.

In this paper, we first propose a method to generate high-charge microbunches with a very large bunching factor, as shown schematically in Fig. 1(a). In this scheme, an electron beam with a charge of nanocoulombs to tens of nanocoulombs [Fig. 1(b)] traverses a plasma section producing a plasma wake. For a bunch with density much higher than the plasma density and length much longer than the plasma wavelength, the longitudinal wakefield  $E_z$  inside the electron beam is approximately a periodic “sawtooth” nonlinear wave [Fig. 1(c)]. Depending on the location along the electron bunch, electrons either gain or lose energy and a “sawtooth” longitudinal energy modulation is induced. At the same time, the transverse wakefield at the cliff of the “sawtooth”—a very small region compared with the wavelength—is defocusing for electrons, resulting in a prebunching effect in the beam [Fig. 1(d)]. After the beam exits the plasma, a chicane is used to further transform the energy modulation into a density modulation. Besides, nearly all electrons in every ramp of the “sawtooth” form a single microbunch without a dc component [Fig. 1(e)]. The bunching factor can thus be significantly increased, leading to a large increase in the terahertz-energy-conversion efficiency. The frequency of the bunch train can be easily tuned by changing the plasma density.

## II. THEORETICAL ANALYSES

To quantify the effectiveness of the above scheme, theoretical analysis is performed with the nonlinear plasma wakefield theory in the blowout regime [29]. We begin by initializing a uniform plasma with density  $n_p$ , and a longitudinally flat-top electron beam with density  $n_b$ , length

$L_b$ , and rms spot size  $\sigma_r$  (transverse Gaussian profile). For an overdense beam ( $n_b > n_p$ ), nonlinear plasma wakes are excited, and according to Ref. [29],  $E_z$  in each transverse slice is found to be proportional to the product of the local radius of the ion channel  $r_b$  and the slope  $dr_b/d\xi$ ; that is,  $E_z(\xi) \approx \frac{1}{2}r_b(dr_b/d\xi)$ , where  $(\xi, r_b)$  are cylindrical coordinates with  $\xi = ct - z$  and the electron beam is moving in the positive  $z$  direction. The shape of the bubble is represented by the trajectory of the innermost particle (see Ref. [29]). For the realistic beam parameters we are interested in, the normalized maximum radius of the ion channel  $k_p r_m \approx 2.58\sqrt{\Lambda} \lesssim 1$  [30], where  $k_p = \sqrt{n_p e^2 / m \epsilon_0 c^2}$  is the plasma wave number and  $\Lambda \equiv \int_0^\infty k_p r(n_b/n_p) dk_p r = (n_b/n_p) k_p^2 \sigma_r^2 = 2I_b/I_A$  is the normalized beam charge per unit length, where  $I_b = Qc/L_b$  is the beam peak current and  $I_A \approx 17$  kA is the Alfvén current.

In this case, the equation for the trajectory of the innermost particle is simplified to (see Ref. [29])

$$\left(1 + \frac{1}{4}r_b^2\right) \frac{d^2 r_b}{d\xi^2} + \frac{1}{2}r_b \left(\frac{dr_b}{d\xi}\right)^2 + \frac{1}{2}r_b = \frac{\lambda(\xi)}{r_b}, \quad (1)$$

where the driving term  $\lambda(\xi) = \Lambda$  in the beam region and  $\lambda(\xi) = 0$  outside the beam region. Here we adopt normalized units, with length normalized to the skin depth  $k_p^{-1}$ , density to the plasma density  $n_p$ , charge to the electron charge  $e$ , and fields to the cold nonrelativistic wave-breaking limit  $E_p = mk_p c^2 / e$ .

Since the bunch length  $L_b$  is much longer than the plasma wavelength, a series of plasma bubbles will be formed along the beam. At each maximum blowout radius  $\xi = \xi_{m,i}$ ,  $r_b = r_m$  and  $dr_b/d\xi = 0$ , where  $i$  is the bubble number. The blowout radius  $r_b(\xi)$  can then be Taylor-expanded about  $\xi = \xi_{m,i}$ :

$$r_b(\xi) \approx r_m + \frac{1}{2} \frac{d^2 r_b}{d\xi^2}(\xi_{m,i})(\xi - \xi_{m,i})^2. \quad (2)$$

This leads to

$$\frac{dr_b}{d\xi} \approx \frac{d^2 r_b}{d\xi^2}(\xi_{m,i})(\xi - \xi_{m,i}) \quad (3)$$

and

$$E_z(\xi) \approx \frac{1}{2}r_b \frac{dr_b}{d\xi} \approx \frac{1}{2}r_m \frac{d^2 r_b}{d\xi^2}(\xi_{m,i})(\xi - \xi_{m,i}). \quad (4)$$

From the equation of motion for  $r_b$  [Eq. (1)],

$$\frac{d^2 r_b}{d\xi^2}(\xi_{m,i}) = -\frac{(1/2) - \lambda(\xi_{m,i})/r_m^2}{1 + (1/4)r_m^2} r_m, \quad (5)$$

the slope of  $E_z$  at  $\xi = \xi_{m,i}$  can be written as

$$\frac{dE_z}{d\xi}(\xi_{m,i}) \approx -\frac{1}{2}r_m^2 \frac{\frac{1}{2} - \lambda(\xi_{m,i})/r_m^2}{1 + \frac{1}{4}r_m^2}. \quad (6)$$

Substituting  $r_m \approx 2.58\sqrt{\Lambda} \approx 2.58\sqrt{2I_b/I_A}$  (normalized to  $k_p^{-1}$ ) into the above expression, we obtain

$$\frac{dE_z}{d\xi}(\xi_{m,i}) \approx -\frac{1.1641\Lambda}{1 + 1.6641\Lambda} \approx -\frac{2.3282I_b}{I_A + 3.3282I_b}. \quad (7)$$

After propagation in the plasma with length  $L_p$ , the accumulated linear energy chirp slope (not normalized, in absolute units) is given by

$$h \approx \frac{-eE_p k_p L_p}{W_i} \frac{dE_z}{d\xi}(\xi_{m,i}) \approx \frac{mc^2 k_p^2 L_p}{W_i} \frac{2.3282I_b}{I_A + 3.3282I_b}, \quad (8)$$

where  $W_i$  is the initial beam energy. Such energy modulation can be transformed into a density modulation in a magnetic chicane. The chicane is composed of a set of four dipole magnets. It is customary to characterize the chicane by its time-of-flight parameter  $R_{56}$ , which defines the path-length difference as a function of the energy offset. To obtain a maximum bunching factor, “full compression” should be achieved, and thus

$$R_{56} = -1/h. \quad (9)$$

The spacing between each bunch equals to energy-modulation wavelength; that is, the plasma-wake wavelength, which is slightly larger than  $2\pi/k_p$  in the nonlinear regime. Therefore, the final radiation frequency can be easily tuned by varying the plasma density.

### III. START-TO-END SIMULATIONS

The scheme proposed above can be implemented in most x-ray-free-electron-laser (FEL) facilities or dedicated small-accelerator facilities. To illustrate its practical validity and examine the theoretical results, we show here one typical example through self-consistent three-dimensional (3D) start-to-end simulations by using a set of well-benchmarked codes. In this example, a 2.5-nC, 135-MeV electron beam with an intrinsic slice energy spread of 0.02 MeV is sent through a plasma section to gain a “sawtooth” energy modulation. Such a modulation is then transformed into a density bunching with a bunching factor as high as 0.8 through a magnetic chicane. The beam has a 5-ps flat-top current profile ( $L_b = 1.5$  mm) with a peak current of  $I_b = 0.5$  kA and normalized emittance  $\epsilon_n = 2$  mm mrad. Such beam parameters are available from the high-brightness injector of some FEL facilities, especially for one driven by a semiconductor photocathode rf gun.

The simulation of the beam passing through the plasma modulator is performed with the particle-in-cell code QUICKPIC [31–33]. Then the beam macroparticles are loaded into the particle-tracking code gpt [34,35] to further track the beam’s six-dimensional phase-space dynamics in the chicane.

As addressed above, the frequency of the bunch train or the final radiation is determined by the plasma-wake wavelength. While terahertz waves of application interest are in the frequency range from 0.1 to 10 THz, here we choose the typical frequency of 1 THz as an example. For other frequencies, similar results can be obtained by scaling the beam and plasma parameters accordingly. To generate a frequency of 1 THz, a nonlinear plasma wake wavelength of  $300 \mu\text{m}$  (1 ps) is required. Therefore, the plasma density is chosen as  $n_p = 1.6 \times 10^{16} \text{ cm}^{-3}$  ( $k_p^{-1} = 42 \mu\text{m}$ ). For a beam density  $n_b$  larger than  $n_p$  to excite a nonlinear plasma wake, the beam is focused to a spot size  $\sigma_r$  of  $5 \mu\text{m}$  at the entrance of the plasma, leading to  $n_b = 6.8 \times 10^{16} \text{ cm}^{-3}$  ( $4.22n_p$ ). Such a small spot size can be achieved with strong focusing elements, such as permanent-magnet quadrupoles, active plasma lenses [36–38], and plasma-matching sections [39]. Details of the QUICKPIC simulation are presented in Figs. 2 and 3. The densities of the plasma and the electron beam are plotted in Fig. 2(a). As shown, the plasma electrons are expelled from a region around the axis by the space charge of the electron beam, leaving behind a column of plasma ions. The expelled, blown-out electrons form a narrow sheath just outside the ion channel with a radius of  $r_b$ . The simulated value of the maximum radius  $r_m$  is  $0.62k_p^{-1}$ , in good agreement with the theoretical value ( $2.58\sqrt{I_b/I_A} = 0.63k_p^{-1}$ ).

The  $E_z$  field in the plasma is shown in Fig. 2(b).  $E_z$  is transversely uniform within the ion channel, leading to a negligible increase of the slice energy spread. The on-axis line out of  $E_z$  [green line in Fig. 2(b)] clearly shows the feature of a “sawtooth” waveform. The simulated value of  $dE_z/d\xi$  at each maximum blowout radius (i.e.,  $r_b = r_m$ ) is  $-0.056mc^2 k_p^2/e$  [see the dashed black line in Fig. 2(b)], which is close to the theoretical value ( $-0.062mc^2 k_p^2/e$ ) according to Eq. (7). The bunch electrons located in the region of negative  $E_z$  slope (i.e.,  $dE_z/d\xi < 0$ ) will gain a positive energy chirp (higher energy at the tail) during propagation in the plasma and then be compressed to form each single microbunch after the chicane, while those located in the region of positive  $E_z$  slope (i.e.,  $dE_z/d\xi > 0$ ) will gain a negative energy chirp (lower energy at the tail) and then be stretched to form the dc component after the chicane. Since the region of negative  $E_z$  slope is much longer than that of positive  $E_z$  slope, most electrons in the bunch finally contribute to the microbunch, while only a small fraction of electrons contribute to the dc component. This will significantly help to increase the bunching factor.

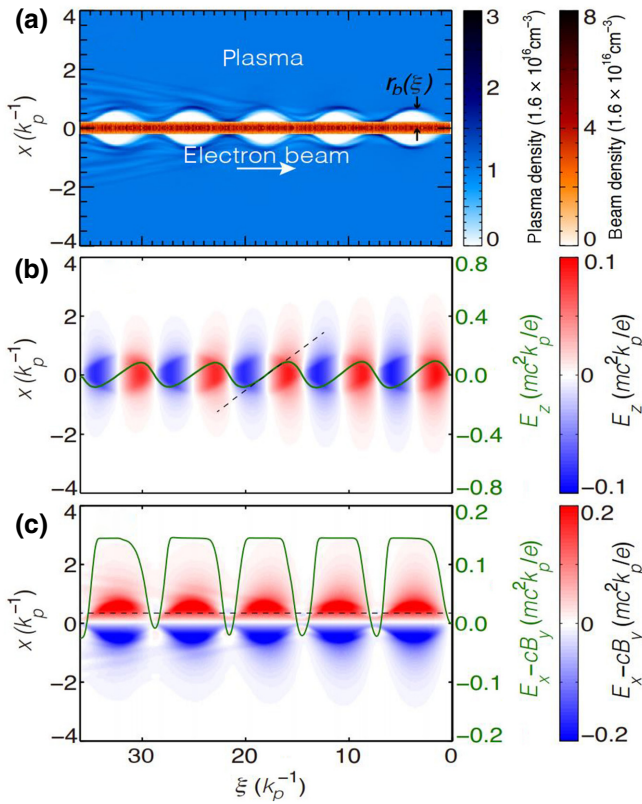


FIG. 2. Three-dimensional particle-in-cell simulation of the beam (propagating to the right) passing through the plasma modulator. (a) The densities of the plasma and the electron beam. The definition of  $r_b$  is also illustrated. (b) The  $E_z$  field excited by the electron bunch. The line out of the on-axis  $E_z$  ( $x = 0 \mu\text{m}$ ,  $\xi$ ) is shown with the solid green line. The dashed black line shows the slope of  $E_z$  at the maximum blowout radius. (c) The transverse wakefield  $W_\perp = E_x - cB_y$  excited by the electron beam. The line out of the off-axis  $W_\perp$  along the dashed black line ( $x = 0.3k_p^{-1}$ ,  $\xi$ ) is shown with the solid green line.

Figure 2(c) shows the transverse wakefields  $W_\perp = E_x - cB_y$ , excited by the electron beam. Within most of the ion channel,  $W_\perp = x/2$  ( $x$  normalized to  $k_p^{-1}$  and  $W_\perp$  normalized to  $mc^2k_p/e$ ) [29]. Such linear focusing force can preserve the emittance of most of the beam. However, in some other region corresponding to positive  $E_z$  slope,  $W_\perp$  decreases and even reverses its sign (defocusing for electrons), as shown in the line out of the off-axis  $W_\perp$  [green line in Fig. 2(c)], leading to different beam transverse dynamics. The output-beam  $p_x$ - $\xi$  phase space for a 3-mm-long plasma is shown in Fig. 3(a). The electrons in the region of positive  $E_z$  slope have a relatively large transverse momentum  $p_x$ , which can be removed during further transport with use of a lead collimator placed between the plasma and the chicane, leading to a prebunching effect. Such an effect will further reduce the dc component after the chicane and increase the bunching factor. Here, by our assuming that electrons with  $|p_x| > 1mc$  can

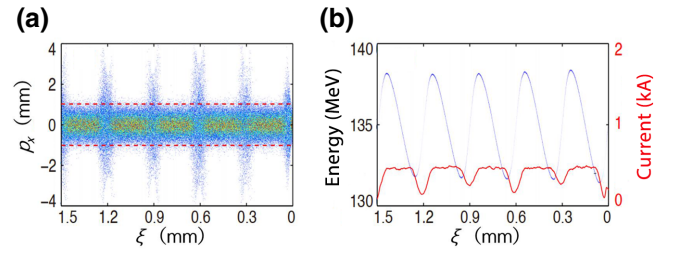


FIG. 3. (a) The beam  $p_x$ - $\xi$  phase space. (b) The beam longitudinal phase space and current profile.

be removed, the charge-loss ratio is relatively low (approximately 20%). The resulting beam longitudinal phase space and current distribution at the entrance of the chicane are presented in Fig. 3(b). The simulated value ( $377.9 \text{ m}^{-1}$ ) of the linear energy-chirp slope  $h$  agrees well with the theoretical value ( $405.1 \text{ m}^{-1}$ ) according to Eq. (8).

Then we use GPT to simulate the beam dynamics in the chicane. Here both the space-charge effect and the coherent-synchrotron-radiation (CSR) effect are considered. The CSR calculation is based on the 3D CSR model [35]. In the simulation, we scan  $R_{56}$  of the chicane (from  $-2.8$  to  $-4$  mm) and find that a bunching factor at the fundamental frequency (1 THz) as high as approximately 0.8 can be obtained over a wide  $R_{56}$  range [Fig. 4(a)], suggesting high robustness of this method. The simulated  $R_{56}$  value of “full compression” is  $-3.0$  mm, in agreement with the theoretical value according to Eq. (9) ( $-2.5$  mm). In this case, the beam longitudinal phase space is given in Fig. 4(b), where each microbunch stands nearly upright, leading to a high peak current. The corresponding current profile is shown in Fig. 4(c). The bunch length of each microbunch reduces to approximately 20 fs (rms) and thus the peak current reaches approximately 10 kA. Figure 4(d) shows the corresponding bunching factor  $b$  at the fundamental and harmonic frequencies, where high  $b$  values of all the fundamental and harmonic frequencies can be clearly seen (e.g.,  $b = 0.78$  at 1 THz and  $b = 0.48$  at 9 THz).

The proposed method is of great advantage in the generation of high-power tunable narrowband terahertz radiation. The final terahertz radiation frequency is approximately proportional to  $k_p \propto \sqrt{n_p}$ ; therefore by variation of  $n_p$ , the terahertz radiation frequency can be conveniently tuned. For example, simulations confirm that by our simply changing  $n_p$  from  $4 \times 10^{15}$  to  $6.4 \times 10^{16} \text{ cm}^{-3}$  while keeping the beam parameters unchanged, a bunching factor of 0.8 can be achieved for a fundamental frequency from 0.5 to 2 THz. For even higher frequencies (e.g., 10 THz), similar results can also be obtained by further increasing  $n_p$  while at the same time reducing the beam transverse size  $\sigma_r$  (e.g., using a plasma-matching section [39] before the plasma modulator) to ensure  $n_b > n_p$  for effectively exciting a nonlinear plasma wake. Since the

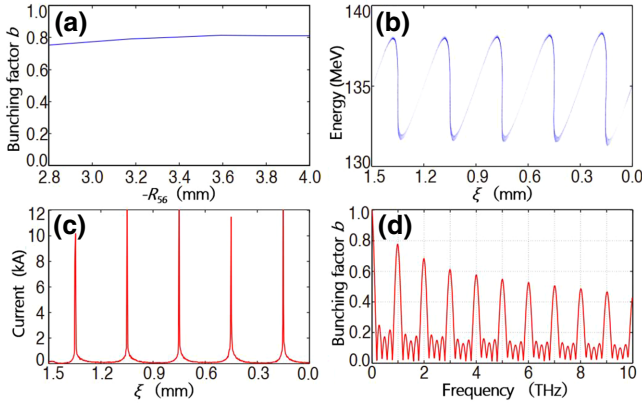


FIG. 4. (a) Bunching factor  $b$  at the fundamental frequency of 1 THz for different  $R_{56}$  values of the chicane. (b) The beam longitudinal phase space for the “full compression” case. (c) The corresponding beam current distribution. (d) The corresponding bunching factors at the fundamental and harmonic frequencies.

medium is a fully ionized plasma and the excited wakefield is a nonlinear wake, such a plasma-modulation technique can sustain high-charge (nanocoulombs to even tens of nanocoulombs) beams.

In addition,  $E_z$  inside the plasma ion channel is transversely uniform, leading to a negligible increase of the slice energy spread, which then determines an extremely short length (approximately 20 fs rms) and a very high peak current (approximately 10 kA, 1 order of magnitude higher than the currents obtained through other methods) of the microbunch. This is helpful for obtaining a large bunching factor at the harmonic frequencies [e.g.,  $b \approx 0.48$  for the ninth harmonic; see Fig. 4(d)]. Furthermore, because of the linear transverse focusing wake in the plasma ion channel, the beam emittance can be preserved for subsequent matching and focusing.

Assuming the bunch train is sent through a helical undulator to emit terahertz radiation, we consider the undulator period  $\lambda_u = 20$  cm and undulator strength  $K = 0.934\lambda_u B_u = 20.4$  to be resonant at 1 THz (radiation wavelength  $\lambda_r = 300 \mu\text{m}$ ), where  $B_u$  is the peak magnetic field. Because the undulator is also a longitudinally dispersive element ( $R_{56} = -2\lambda_u N_u$ , with  $N_u$  the number of undulator periods), this will cause overcompression or debunching of a fully compressed electron beam as it traverses the undulator, leading to a reduction in the bunching factor and thus the output terahertz energy. Such a debunching rate is positively correlated with the beam energy spread. To reduce the debunching rate and obtain a high average bunching factor within the undulator, the plasma length is shortened from 3 to 0.6 mm [compared with the simulation parameters corresponding to Fig. 3(b)] such that the beam energy spread is reduced fivefold and the beam is undercompressed in the chicane to obtain a bunching factor of approximately 0.6 at the entrance of the undulator [see the

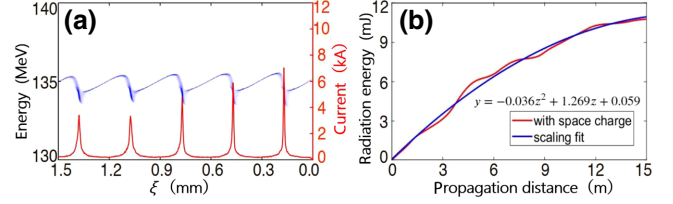


FIG. 5. (a) The beam longitudinal phase space and the corresponding beam current distribution at the entrance of the undulator. (b) The radiation energy versus the propagation distance within the undulator.

simulated longitudinal phase space obtained with QUICKPIC and GPT (including both space-charge and CSR effects) in Fig. 5(a)]. As the beam propagates in the undulator, it will be first further compressed to the full-compression case and then overcompressed. Note that quadrupoles are inserted between the plasma and the chicane, and also between the chicane and the undulator to match the beam. The simulation of the bunch trains passing through the undulator is done with the well-benchmarked code GENESIS [40], which is a time-dependent 3D FEL code modeling the radiation field and the electron beam, including both the longitudinal and the transverse effects. In the GENESIS simulations, we turn on the space-charge module.

Simulation results show that with a 10-m-long undulator ( $N_u = 50$ ), the emitted terahertz pulse energy is about 9 mJ [Fig. 5(b)]. If the undulator length is further increased to 15 m, the radiation energy can reach approximately 11 mJ. Furthermore, the radiation is highly directional, which is beneficial for further revolutionizing science applications. With repetition rates on the order of kilohertz or submegahertz for both the accelerator (using a superconducting linac) and the plasma source (using either a capillary-discharge waveguide [41] or a continuous-flow gas jet [42]), future coherent terahertz sources with an average power of 10 W or even kilowatts could be realized.

#### IV. CONCLUSION

In summary, we propose a method based on nonlinear plasma wakefield modulation to generate extremely strong density bunching in a high-charge relativistic electron beam. Theoretical analysis and start-to-end simulations show that the combination of a plasma modulator and a chicane with proper parameters can generate microbunch trains with high charge of up to a few nanocoulombs and a bunching factor as high as approximately 0.8, which can be used to produce tunable intense narrowband terahertz radiation with energy on the order of 10 mJ. The high spectral brightness of the radiation makes it a powerful and promising method for many forefront scientific applications.

## ACKNOWLEDGMENTS

This work was supported by the National Natural Science Foundation of China (Grant No. 11835004) and by China Science Challenge Project (Grant No. TZ2018005).

- 
- [1] Emilio A. Nanni, Wenqian R. Huang, Kyung-Han Hong, Koustuban Ravi, Arya Fallahi, Gustavo Moriena, R. J. Dwayne Miller, and Franz X. Kärtnerothers, Terahertz-driven linear electron acceleration, *Nat. Commun.* **6**, 8486 (2015).
- [2] P. H. Siegel, Terahertz technology, *IEEE Trans. Microw. Theory Tech.* **50**, 910 (2002).
- [3] Mengkun Liu, Harold Y. Hwang, Hu Tao, Andrew C. Strikwerda, Kebin Fan, George R. Keiser, Aaron J. Sternbach, Kevin G. West, Salinporn Kittiwatanakul, and Jiwei Lu, *et al.*, Terahertz-field-induced insulator-to-metal transition in vanadium dioxide metamaterial, *Nature* **487**, 345 (2012).
- [4] Tobias Kampfrath, Koichiro Tanaka, and Keith A. Nelson, Resonant and nonresonant control over matter and light by intense terahertz transients, *Nat. Photonics* **7**, 680 (2013).
- [5] Yuelin Li, Kwang-Je Kim, Nonrelativistic electron bunch train for coherently enhanced terahertz radiation sources, *Appl. Phys. Lett.* **92**, 014101 (2008).
- [6] Yuzhen Shen, Xi Yang, G. L. Carr, Yoshiteru Hidaka, James B. Murphy, and Xijie Wang, Tunable Few-Cycle and Multicycle Coherent Terahertz Radiation from Relativistic Electrons, *Phys. Rev. Lett.* **107**, 204801 (2011).
- [7] P. Musumeci, R. K. Li, and A. Marinelli, Nonlinear Longitudinal Space Charge Oscillations in Relativistic Electron Beams, *Phys. Rev. Lett.* **106**, 184801 (2011).
- [8] Zhen Zhang, Lixin Yan, Yingchao Du, Zheng Zhou, Xiaolu Su, Lianmin Zheng, Dong Wang, Qili Tian, Wei Wang, and Jiaru Shi, *et al.*, Tunable High-Intensity Electron Bunch Train Production Based on Nonlinear Longitudinal Space Charge Oscillation, *Phys. Rev. Lett.* **116**, 184801 (2016).
- [9] G. Zhao, S. Zhao, S. Huang, and K. Liu, Strong electron density modulation with a low-power thz source for generating thz superradiant undulator radiation, *Phys. Rev. Accel. Beams* **22**, 60701 (2019).
- [10] P. Muggli, V. Yakimenko, M. Babzien, E. Kallos, and K. P. Kusche, Generation of Trains of Electron Microbunches with Adjustable Subpicosecond Spacing, *Phys. Rev. Lett.* **101**, 054801 (2008).
- [11] Y.-E. Sun, P. Piot, A. Johnson, A. H. Lumpkin, T. J. Maxwell, J. Ruan, and R. Thurman-Keup, Tunable Subpicosecond Electron-Bunch-Train Generation Using a Transverse-To-Longitudinal Phase-Space Exchange Technique, *Phys. Rev. Lett.* **105**, 234801 (2010).
- [12] H. Zhang, I. V. Konoplev, and J. Smith, Concept of a tunable source of coherent THz radiation driven by a plasma modulated electron beam, *Phys. Plasma* **25**, 043111 (2018).
- [13] S. Antipov, C. Jing, M. Fedurin, W. Gai, A. Kanareykin, K. Kusche, P. Schoessow, V. Yakimenko, and A. Zholents, Experimental Observation of Energy Modulation in Electron Beams Passing Through Terahertz Dielectric Wakefield Structures, *Phys. Rev. Lett.* **108**, 144801 (2012).
- [14] K. L. F. Bane and G. Stupakov, Terahertz radiation from a pipe with small corrugations, *Nucl. Instrum. Methods Phys. Res., Sect. A* **677**, 67 (2012).
- [15] S. Antipov, M. Babzien, C. Jing, M. Fedurin, W. Gai, A. Kanareykin, K. Kusche, V. Yakimenko, and A. Zholents, Subpicosecond Bunch Train Production for a Tunable mJ Level THz Source, *Phys. Rev. Lett.* **111**, 134802 (2013).
- [16] G. Andonian, S. Barber, F. H. O'Shea, M. Fedurin, K. Kusche, C. Swinson, and J. B. Rosenzweig, Generation of Ramped Current Profiles in Relativistic Electron Beams Using Wakefields in Dielectric Structures, *Phys. Rev. Lett.* **118**, 054802 (2017).
- [17] F. Lemery, G. Amatuni, P. Boonpornprasert, Y. Chen, and J. Good, *et al.*, Passive Ballistic Microbunching of Nonultra-relativistic Electron Bunches Using Electromagnetic Wakefields in Dielectric-Lined Waveguides, *Phys. Rev. Lett.* **122**, 044801 (2019).
- [18] D. Xiang and G. Stupakov, Enhanced tunable narrow-band thz emission from laser-modulated electron beams, *Phys. Rev. Spec. Topics-Accel. Beams* **12**, 080701 (2009).
- [19] Michael Dunning, C. Hast, E. Hemsing, K. Jobe, D. McCormick, J. Nelson, T. O. Raubenheimer, K. Soong, Z. Szalata, and D. Walz, *et al.*, Generating Periodic Terahertz Structures in a Relativistic Electron Beam Through Frequency Down-Conversion of Optical Lasers, *Phys. Rev. Lett.* **109**, 074801 (2012).
- [20] Zhen Wang, Dazhang Huang, Qiang Gu, Zhentang Zhao, and Dao Xiang, Echo-enabled tunable terahertz radiation generation with a laser-modulated relativistic electron beam, *Phys. Rev. Spec. Topics-Accel. Beams* **17**, 090701 (2014).
- [21] Z. Zhang, L. Yan, Y. Du, W. Huang, C. Tang, and Z. Huang, Generation of high-power, tunable terahertz radiation from laser interaction with a relativistic electron beam, *Phys. Rev. ST Accel. Beams* **20**, 050701 (2017).
- [22] Jerry L. LaRue, Tetsuo Katayama, Aaron Lindenberg, Alan S. Fisher, Henrik Öström, Anders Nilsson, and Hirohito Ogasawara, Thz-Pulse-Induced Selective Catalytic CO Oxidation on Ru, *Phys. Rev. Lett.* **115**, 036103 (2015).
- [23] Xi Cheng Zhang, Alexander Shkurinov, and Yan Zhang, Extreme terahertz science, *Nat. Photonics* **11**, 16 (2017).
- [24] Lingrong Zhao, *et al.*, Terahertz Streaking of Few-Femtosecond Relativistic Electron Beams, *Phys. Rev. X* **8**, 021061 (2018).
- [25] Catherine Kealhofer, Waldemar Schneider, Dominik Ehberger, Andrey Ryabov, Ferenc Krausz, and Peter Baum, All-optical control and metrology of electron pulses, *Science* **352**, 429 (2016).
- [26] Dongfang Zhang, Arya Fallahi, Michael Hemmer, Xiaojun Wu, Moein Fakhari, Yi Hua, Huseyin Cankaya, Anne-Laure Calendron, Luis E. Zapata, and Nicholas H. Matlis, *et al.*, Segmented terahertz electron accelerator and manipulator (steam), *Nat. Photonics* **12**, 336 (2018).
- [27] Emma Curry, S. Fabbri, J. Maxson, P. Musumeci, and A. Gover, Meter-Scale Terahertz-Driven Acceleration of a Relativistic Beam, *Phys. Rev. Lett.* **120**, 094801 (2018).
- [28] Peter Weightman, Prospects for the study of biological systems with high power sources of terahertz radiation, *Phys. Biol.* **9**, 053001 (2012).

- [29] W. Lu, C. Huang, M. Zhou, W. B. Mori, and T. Katsouleas, Nonlinear Theory for Relativistic Plasma Wakefields in the Blowout Regime, *Phys. Rev. Lett.* **96**, 165002 (2006).
- [30] W. Lu, C. Huang, M. Zhou, and M. Tzoufras, A nonlinear theory for multidimensional relativistic plasma wave wakefields, *Phys. Plasma* **13**, 056709 (2006).
- [31] C. Huang, V. K. Decyk, M. Zhou, W. Lu, W. B. Mori, J. H. Cooley, T. M. Antonsen Jr., B. Feng, T. Katsouleas, and J. Vieira, Quickpic: A highly efficient fully parallelized PIC code for plasma-based acceleration, *J. Phys. Confer. Ser.* **46**, 190 (2006).
- [32] W. An, V. K. Decyk, W. B. Mori, and T. M. Antonsen Jr., An improved iteration loop for the three dimensional quasi-static particle-in-cell algorithm: Quickpic, *J. Comput. Phys.* **250**, 165 (2013).
- [33] Quickpic open source, <https://github.com/UCLA-Plasma-Simulation-Group/QuickPIC-OpenSource>.
- [34] S. B. Van der Geer, and M. J. de Loos, in *Proc. 6th European Particle Accelerator Conference* (Joint Accelerator Conferences Website (JACoW), Stockholm, Sweden, 1998).
- [35] A. D. Brynes, P. Smorenburg, I. Akkermans, E. Allaria, L. Badano, and S. Brussaard, *et al.*, Beyond the limits of 1d coherent synchrotron radiation, *New J. Phys.* **20**, 073035 (2018).
- [36] J. van Tilborg, S. Steinke, C. G. R. Geddes, N. H. Matlis, B. H. Shaw, A. J. Gonsalves, J. V. Huijts, K. Nakamura, J. Daniels, C. B. Schroeder, C. Benedetti, E. Esarey, S. S. Bulanov, N. A. Bobrova, P. V. Sasorov, and W. P. Leemans, Active Plasma Lensing for Relativistic Laser-Plasma-Accelerated Electron Beams, *Phys. Rev. Lett.* **115**, 184802 (2015).
- [37] R. Pompili, *et al.*, Focusing of High-Brightness Electron Beams with Active-Plasma Lenses, *Phys. Rev. Lett.* **121**, 174801 (2018).
- [38] C. A. Lindström, E. Adli, G. Boyle, R. Corsini, A. E. Dyson, W. Farabolini, S. M. Hooker, M. Meisel, J. Osterhoff, J.-H. Röckemann, L. Schaper, and K. N. Sjobak, Emittance Preservation in an Aberration-Free Active Plasma Lens, *Phys. Rev. Lett.* **121**, 194801 (2018).
- [39] X. Xu, J. Hua, Y. Wu, C. Zhang, F. Li, Y. Wan, C. Pai, W. Lu, W. An, and P. Yu, *et al.*, Physics of Phase Space Matching for Staging Plasma and Traditional Accelerator Components Using Longitudinally Tailored Plasma Profiles, *Phys. Rev. Lett.* **116**, 124801 (2016).
- [40] S. Reiche, Genesis 1.3: A fully 3D time-dependent FEL simulation code, *Nucl. Instrum. Methods Phys. Res., Sect. A* **429**, 243 (1999).
- [41] A. J. Gonsalves, F. Liu, N. A. Bobrova, P. V. Sasorov, C. Pieronek, J. Daniels, S. Antipov, J. E. Butler, S. S. Bulanov, W. L. Waldron, D. E. Mittelberger, and W. P. Leemans, Demonstration of a high repetition rate capillary discharge waveguide, *J. Appl. Phys.* **119**, 033302 (2016).
- [42] L. Rovige, J. Huijts, I. Andriyash, A. Vernier, and J. Faure, Demonstration of stable long-term operation of a kilohertz laser-plasma accelerator, *Phys. Rev. Accel. Beams* **23**, 093401 (2020).